Journal of Hazardous Materials 484 (2025) 136760

Contents lists available at ScienceDirect

Journal of Hazardous Materials

journal homepage: www.elsevier.com/locate/jhazmat

Chemoproteomic profiling by bioorthogonal probes to reveal the novel targets of acrylamide in microglia

Binru Zheng [a], Jia Shang [a,1], Yuanqing Wei [a,1], Qianqian Tao [a], Jizhou Yin [a], An Kang [a], Rui Liu [a,b,c,*], Hongzhen Lian [d,**], Shuying Han [a,**]

[a] College of Pharmacy, Nanjing University of Chinese Medicine, Nanjing 210023, China
[b] National and Local Collaborative Engineering Center of Chinese Medicinal Resources Industrialization and Formulae Innovative Medicine, Jiangsu Collaborative Innovation Center of Chinese Medicinal Resources Industrialization, Key Laboratory of Chinese Medicinal Resources Recycling Utilization under National Administration of Traditional Chinese Medicine, Nanjing University of Chinese Medicine, Nanjing 210023, China
[c] Jiangsu Key Laboratory of Research and Development in Marine Bio-resource Pharmaceutics, Nanjing University of Chinese Medicine, Nanjing 210023, China
[d] State Key Laboratory of Analytical Chemistry for Life Science, School of Chemistry & Chemical Engineering and Center of Materials Analysis, Nanjing University, Nanjing 210023, China

HIGHLIGHTS

- The synthesized probe AAPA-P2 can profile acrylamide targets directly in living cells.
- The identified number of proteins after enrichment with AAPA-P2 was increased 20-fold.
- Novel targets reveal AA promotes apoptosis through PSMD9/NDUFA5/ Caspase 3 pathway.

GRAPHICAL ABSTRACT

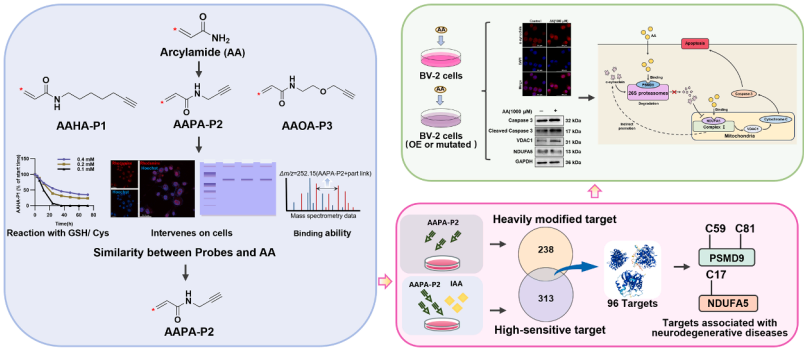

ARTICLE INFO

Keywords:
Acrylamide
Neurotoxicity
Covalent binding sites
Bioorthogonal probe

ABSTRACT

Neurotoxicity studies caused by exposure to acrylamide (AA) are of wide interest, but the methods for direct analysis of AA targets in living neuronal cells by cysteine profiling are still lacking. To address this, we developed a specific bioorthogonal probe, AAPA-P2, for chemical proteomics analysis of AA covalent binding sites. AAPA-P2 captured 754 target proteins, increasing the number of identified target proteins by 20-fold. Further screening revealed 96 proteins that are both highly sensitive and heavily modified by AAPA-P2, with validation performed on some potential key targets and binding sites. AA was found to induce neurotoxicity by binding to newly identified targets, Proteasome 26S Subunit, non ATPase 9 (PSMD9) and NADH dehydrogenase (ubiquinone) 1 alpha subcomplex 5 (NDUFA5), interfering with the ubiquitin-proteasome system, and inducing mitochondria-dependent apoptosis. The present work provides an effective bioorthogonal probe tool for identifying covalent

* Corresponding author at: College of Pharmacy, Nanjing University of Chinese Medicine, Nanjing 210023, China.
** Corresponding authors.
E-mail addresses: liurui@njucm.edu.cn (R. Liu), hzlian@nju.edu.cn (H. Lian), syhan@njucm.edu.cn (S. Han).
[1] Co-first authors.

https://doi.org/10.1016/j.jhazmat.2024.136760
Received 29 June 2024; Received in revised form 23 November 2024; Accepted 2 December 2024
Available online 4 December 2024

binding targets of acrylamide and offers new insights into the molecular mechanisms underlying acrylamide-induced neurotoxicity.

1. Introduction

Acrylamide (AA) is a water-soluble vinyl monomer with a variety of chemical and industrial applications [1]. In a report by the International Agency for Research on Cancer (IARC) in 1994, AA was classified as a Group 2a substance, indicating that it is possibly carcinogenic to humans and a neurotoxin [2]. Previously, it was generally believed that the primary risks associated with AA were due to occupational exposure, as polyacrylamide has been widely used since the 1950s for soil conditioning, wastewater treatment, cosmetics, and papermaking [3–6]. However, recent concerns have emerged regarding the presence of AA in food and its impact on human health. The main source of AA in food comes from the high-temperature cooking and processing of starchy foods, where free asparagine and reducing sugars in these foods (especially potatoes, baked goods, plant-derived products, and coffee) undergo the Maillard reaction at elevated temperatures to produce AA [7]. Mihalache OA applied risk assessment methods to evaluate the risk of cancer and disease burden associated with dietary exposure to AA through exposure models [8]. It was also reported that AA can affect steroid hormone levels during adolescence, leading to reproductive neuroendocrine toxicity [9]. Additionally, research by Guo J has demonstrated that men and individuals under 65 years old are more susceptible to depression after environmental exposure to AA [10].

Currently, preliminary studies have been conducted on the toxic mechanisms of acrylamide. As an electrophilic reagent containing an α,β-unsaturated amide group, AA can modify nucleophilic residues of macromolecules, particularly cysteine (Cys) residues through Michael addition, resulting in a process known as “acrylamidation”, which interferes with the biological functions of these molecules and leads to neurotoxicity, skeletal developmental toxicity and carcinogenicity [11–17]. However, existing studies still face several bottlenecks, the main challenge of which is the limited understanding of the target proteins of AA. Mass spectrometry (MS)-based proteomics techniques are increasingly used for screening target proteins of drugs/toxins, and studies have shown that AA can modify approximately 200 proteins in different types of nerve cells [18–22], however, these targets are predominantly high-abundance proteins, while low-abundance target proteins with high activity are difficult to detect due to their low expression levels in living cells [23–25]. Current target identification methods struggle to provide a comprehensive description of the proteins that bind with AA, resulting in the omission of critical information related to the molecular mechanisms of AA-induced neurotoxicity. Thus, new research tools and methods capable of covering both a global portrait of AA reactivity and direct analysis of protein-specific sites in living cells are highly desired.

To address this issue, we designed and synthesized a bioorthogonal probe structurally similar to AA, named AAPA-P2 in this work. Utilizing this probe, 754 AA-modified proteins were captured and identified in mouse microglia cells (BV-2) cells, significantly increasing the number of identified proteins compared to traditional proteomics methods. Further screening and analysis of these binding proteins revealed that AA can induce neuronal apoptosis through covalent binding to Cys59 of PSMD9 and Cys17 of NDUFA5. This research provides a wealth of target protein information and new insights for subsequent studies on the molecular mechanisms of AA-induced neurotoxicity, as well as potential therapeutic targets for treating AA-related neural damage.

2. Materials and methods

2.1. Chemicals and reagents

All reagents, antibodies, primers, plasmids and methods and procedures that are not mentioned in the main text are all presented in the Supporting Information.

2.2. Compound synthesis

N-6-heptyn-1-yl-2-propenamide (AAHA-P1) was synthesized according to the following method. 10 mmol 6-heptyn-1-amine HCl and 25 mmol 4-dimethylaminopyridine were dissolved in 80 mL distilled CH_2Cl_2. The reaction mixture was stirred at room temperature for 4–5 h. To this solution, 11 mmol of acryloyl chloride diluted in CH_2Cl_2 was added dropwise under cooling in an ice bath. The reaction mixture was stirred at −5 °C for 30 min and at room temperature for another 12–16 h. After removing most of the solvent by evaporation at reduced pressure, the residue mixture was separated on a silica column to afford AAHA-P1 as a yellow powder.

N-(prop-2-ynyl)acrylamide (AAPA-P2) was synthesized according to the following method. 10 mmol propargyl amine and 15 mmol 4-dimethylaminopyridine were dissolved in 80 mL distilled CH_2Cl_2. To this solution, 11 mmol of acryloyl chloride diluted in CH_2Cl_2 was added dropwise under cooling in an ice bath. The reaction mixture was stirred at −5 °C for 30 min and at room temperature for another 12–16 h. After removing most of the solvent by evaporation at reduced pressure, the residue mixture was separated on a silica column to afford AAPA-P2 as a yellow powder.

N-(2-(prop-2-yn-1-yloxy)ethyl)acrylamide (AAOA-P3) was synthesized according to the following method. 10 mmol 2-(2-propynyloxy) ethylamine and 15 mmol 4-dimethylaminopyridine were dissolved in 80 mL distilled CH_2Cl_2. To this solution, 11 mmol of acryloyl chloride diluted in CH_2Cl_2 was added dropwise under cooling in an ice bath. The reaction mixture was stirred at −5 °C for 30 min and at room temperature for another 12–16 h. After removing most of the solvent by evaporation at reduced pressure, the residue mixture was separated on a silica column to afford AAOA-P3 as a yellow powder.

2.3. Cell culture

BV-2, rat pheochromocytoma cells (PC12) and human neuroblastoma cells (SHSY-5Y) were obtained from American Type Culture Collection (ATCC) and maintained in DMEM (Pricella, Wuhan, Hubei, China, WH0023Z281) supplemented with 10 % (vol/vol) dialyzed FBS (Pricella, SA220822), 100 U mL^{-1} penicillin and 100 mg mL^{-1} streptomycin in a humidified atmosphere at 37 °C with 5 % CO_2.

2.4. Cell viability assays

For evaluation of the cell toxicity of AA, AAHA-P1, AAPA-P2 and AAOA-P3, 10,000 BV-2 cells per well were seeded in 96-well dishes to grow 24 h. Then the cells were treated with 50, 100, 200, 400, 800, 1000, 2000 μM AA or AAHA-P1, AAPA-P2 and AAOA-P3 for 24 h. The cells were washed with pre-warmed PBS (pH=7.2–7.4) and incubated with pre-prepared CCK-8 reagent for 2 h. The absorbance at 450 nm was measured and cell viability under test conditions was reported as a percentage relative to the negative control treatment.

2.5. qRT-PCR

The BV-2 cells were seeded in 6-well plates at 8×10^5 cells/well for 24 h, then stimulated with 100, 400, 1000, 2000 μM AA or AAHA-P1, AAPA-P2 and AAOA-P3 respectively. After 24 h, the cells were washed with PBS three times. Total RNA was isolated and cDNA was synthesized using a Hiscript® II Q RT SuperMix for qPCR (+gDNA wiper). Quantitative real-time (qRT)-PCR was performed using the ChamQ SYBR qPCR Master Mix (Without ROX). The primer sequences are listed in Table S1 in the Supporting information. The results were analyzed by the ®$2^{-\Delta\Delta t}$ method using β-actin for normalization.

2.6. Activity-based protein profiling (ABPP)

The BV-2 cells were grown to 80 % confluence. The cells were treated with 100, 400, 1000 μM of AA, or AAHA-P1, AAPA-P2, and AAOA-P3 respectively for 12 h. The cells were washed with PBS for three times and centrifuged at 2500 g for 5 min. The cell pellets were resuspended in ice-cold PBS buffer containing EDTA-free protease inhibitor cocktail. The cells were lysed by sonication in the ice and cell lysates were collected by centrifugation (12000 rpm, 20 min) at 4 °C to remove the debris. The protein concentration was determined by using the BCA protein assay kit. For visualizing the probe labeling efficiency by in-gel fluorescence, 0.5 mL of lysates (1 mg mL^{-1}) were mixed with 5×10^4 μM $CuSO_4$, 5×10^3 μM TBTA, 50 μM TAMRA-azide and 5×10^4 μM TCEP at room temperature for 2 h. The reacted samples were resolved on 10 % SDS-PAGE gels and imaged by ChemiDoc XRS+ (Bio-Rad Laboratories, CA, USA). The gels were then stained by coomassie brilliant blue to demonstrate equal loading.

2.7. IAA competition experiments

The BV-2 cells were grown to 80 % confluence in 10 cm dish. BV-2 cells were treated with 1000 μM AAPA-P2 for 24 h. The cells were collected by PBS wash for three times and centrifugation at 2500 g for 5 min. The cells were lysed in 1.5 mL ice-cold PBS buffer containing EDTA-free protease inhibitor cocktail with sonication. The cell lysates were collected by centrifugation (12000 rpm, 20 min) at 4 °C to remove the debris. The protein concentration was determined by using the BCA protein assay kit. 3 mL cell lysates (1 mg mL^{-1}) were incubated with 0.20 mmol IAA. The rest of the operation was as above.

2.8. Western blot (WB)

Proteins were extracted with RIPA buffer supplemented with 1 × protease inhibitor cocktail and separated on SDS-PAGE gel, followed by electro-transferring to PVDF membranes. Next, samples were incubated with the corresponding primary antibodies (listed in the section of Antibodies and reagents.) and secondary antibody. The protein band was visualized using enzyme-linked chemiluminescence reagent in Tanon automatic chemiluminescence image analysis system (Shanghai, China). The protein amount was semi-quantified by Image J, and normalized to its corresponding control.

2.9. Immunofluorescence (IF)

The BV-2 cells were fixed with 4 % paraformaldehyde in PBS overnight at 4 °C and permeabilized with 0.2 % Triton X-100 in PBS for 15 min at room temperature. The cells were blocked with 5 % bovine serum albumin (Sigma) for 30 min and incubated with an anti-NDUFA5 antibody (listed in the section of Antibodies and reagents.) diluted in PBS containing 0.2 % bovine serum albumin for 2 h at room temperature. After washing three times with PBS, the cells were incubated with fluorescent isothiocyanate-conjugated goat anti-rabbit IgG for 1 h at room temperature. Thereafter, the cells were stained with 4′,6-diamidino-2-phenylindole (1 mg mL^{-1}) for 15 min and observed under an inverted fluorescence microscope (Leica TCS SP8, Germany).

2.10. LC-MS/MS analysis

The sample was diluted to a 1 mM solution prior to analysis by LC-MS/MS on Q Dionex Ultimate 3000 nanoLC system (Thermo Scientific, Waltham, MA, USA) coupled to a Q Exactive Plus Orbitrap Mass Spectrometer (Thermo). Under the positive ion mode, full-scan mass spectra were acquired over the m/z range from 300 to 2000. The samples in 0.1 % formic acid were directly loaded and separated at a flow rate of 400 nL min^{-1} on a lab-fabricated RP capillary column (75 μm × 15 cm, particle size 3 μm) with 0.2 % formic acid in 98 % water (solvent A) and 0.2 % formic acid in 80 % ACN (solvent B) as mobile phases. Then the samples were separated using a gradient of solvent B increasing from 2 % to 30 % over 90 min

2.11. Data analysis

All the raw MS/MS data was searched and analyzed using Maxquant software. Tandem mass spectra were searched against the Uniprot_Mus Musculus database (downloaded on March 10, 2022). The oxidation of methionine residues (+15.99 Da), N-terminal acetylation (+42.01 Da), amino formylation (+43.01 Da), as well as + 252.16 Da on cysteine were set as variable modifications. The scores obtained under the above retrieval conditions are significant ($p < 0.05$).

3. Results

3.1. Synthesis of probes

Allowing covalent modification of thiol-containing target proteins by Michael addition, we hypothesized that bioorthogonal probes retaining α,β-unsaturated carbonyl groups should have thiol reactivity similar to that of AA. Therefore, acrylamide-alkynes were designed to mimic AA as closely as possible and the alkyne group was installed in a position that does not interfere with its normal physiological function. Considering the solubility and the permeability of cell membrane of the probe, AAHA-P1, AAPA-P2 and AAOA-P3 were designed and synthesized (Fig. 1 and Supplementary Fig. S1). The ^{1}H NMR, ^{13}C NMR and MS/MS data all confirmed the structures of the designed probes (Supplementary Fig. S2–4).

3.2. Evaluation of the similarity of probes to AA

The reactions of the probes and AA with Cys and glutathione (GSH) were evaluated by LC-MS (Supplementary Fig. S5) and HPLC (Supplementary Fig. S6), respectively, to compare the similarity between the reactions of the synthetic probes and AA with Cys residues. The MS1 and MS2 spectra of these adducts indicated that all the three probes have the same nucleophilic ability as AA to undergo Michael addition reactions with sulfhydryl group. In addition, the reaction kinetic curves and its relevant statistical analysis show that these three probes preserved similar Cys and GSH reactivity as that of AA. AAPA-P2 and AA showed highly similar binding ability to Cys at a concentration of 0.2 mM (mean relative error of 7.42 %), while in the reaction kinetics of GSH, AAOA-P3 showed a high similarity with AA (mean relative error of 9.16 %) at 0.2 mM (Supplementary Table S2).

The functional similarity of the probes to AA in BV-2 cells was then compared. Similar as AA, no obvious cytotoxicity was observed when BV-2 cells were treated with 50, 100, 200, 400, 800, and 1000 μM probes for 24 h. While the concentrations of both AA and probes reached 2000 μM, significant cytotoxicity was observed (Supplementary Fig. S7). All of three probes could notably triggered the release of proinflammatory cytokines including tumor necrosis factor-α (TNF-α), interleukin-1β (IL-1β) and interleukin-6 (IL-6) with similar potency as AA. Likewise, both the probes and AA upregulated the proinflammatory

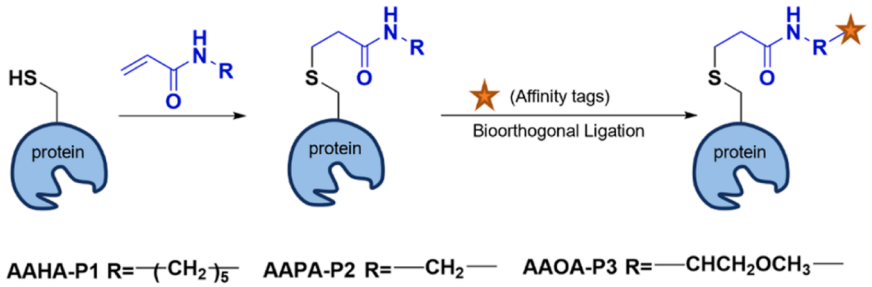

Fig. 1. Design of probes to capture the acrylamide targets: the structures of AAHA-P1, AAPA-P2 and AAOA-P3 are presented.

mediator cyclooxygenase-2 (COX-2), which further promoted neuroinflammation. AAPA-P2 showed the closest potency to AA in promoting the secretion of these proinflammatory cytokines compared to AAHA-P1 and AAOA-P3, with a mean relative error of 7.25 % (Fig. 2A and Supplementary Table S3).

Next, the ability of the probe to specifically label acrylamide targets in living BV-2 cells was assessed. As expected, proteomic analysis of BV-2 cells treated with probes or AA revealed that the reactivity of AAPA-P2 and cysteine residues in the proteins was similar to that of AA (Supplementary Fig. S8). Approximately 77 proteins modified by AA and 38 proteins modified by AAPA-P2 were identified, most of which contained cysteine residues. In contrast, AAHA-P1 and AAOA-P3 synthesized with longer carbon chain "tails" showed significantly different proteomic results, with only about 10 modified peptides being identified. In addition, ABPP technique was used to evaluate the ability of AAHA-P1, AAPA-P2 and AAOA-P3 to enrich and modify peptides. 1251 proteins modified by AAPA-P2, 483 proteins by AAHA-P1, and 231 proteins by AAOA-P3 were identified. The confocal results visually confirmed that AAPA-P2 intracellularly labeled the target proteins to the highest degree compared to the other two probes (Supplementary Fig. S8). The labeling performance of three probes in BV-2 live cells were also investigated. As show in Fig. 3A-B, AAPA-P2 and AA have mutual competition in a concentration-dependent manner. Although AAHA-P1 or AAOA-P3 can also compete with AA in a concentration-dependent manner (Supplementary Fig. S9), they labeled much less proteins than AAPA-P2, which is consistent with the confocal results (Supplementary Fig. S10).

Concentration- and time-dependent labeling showed that treatment with 1000 μm AAPA-P2 for 24 h produced sufficient labeling (Fig. 3A-C). As speculated, AAPA-P2 labeling received intense competition from AA but not from the non-reactive propionamide. Meanwhile, pent-4-ynamide did not induce any protein labeling in living BV-2 cells, confirming that the labeling with AAPA-P2 did not come from its alkynyl metabolites (Fig. 3D). Moreover, AAPA-P2 could also label SH-SY5Y and PC12 with similar efficiency (Fig. 3E).

3.3. Identification of potential target proteins for AA

AAPA-P2 combined with ABPP method were used to identify and quantify AA targets in BV-2 cells (Fig. 4A, Supplementary Table S4 and 5). A total of 754 proteins were obtained by comparing the AAPA-P2 group with dimethyl sulfoxide (DMSO) group and designating proteins with $p < 0.05$ in all the three biological replicates as the creditable AA targets (Supplementary Table S4). In contrast, only 37 modified proteins were detected after treated with AA. The number of AAPA-P2-modified proteins detected after enrichment was 20 times higher than that before enrichment. Among the 37 proteins, 35 were included in the 754 proteins enriched with AAPA-P2 characteristic modification, accounting for 94.6 %. The new dataset covers many targets with AA modification, including peroxiredoxin 5 (PRDX5), ANXA1, histone deacetylase 1 (HDAC1), ubiquitin carboxyl terminal hydrolase L1 (UCHL1), PSMD9, NDUFA5 and TPI1, etc.

To further identify targets that are more sensitive to AA, iodoacetamide (IAA), an alkylation reagent, was used to positively compete with AAPA-P2-labeled target proteins. Treatment of BV-2 cells with 1000 μM AAPA-P2 for 24 h followed by incubation with 20 μM IAA for 30 min resulted in a significant reduction in proteomic labeling of AAPA-P2 (Fig. 4B). It is reasonable to assume that those target proteins that remain AAPA-P2-labeled after competition with IAA are more sensitive acrylamide targets. In this way, 238 proteins were screened out and assigned as high-sensitive acrylamide targets (Fig. 4C and Supplementary Table S6). Satisfyingly, high-sensitive AA targets were highly enriched in bioprocesses including glutathione metabolic process and response to hydrogen peroxide (Fig. 4D).

3.4. NDUFA5 and PSMD9 are potential new targets of AA-induced neurotoxicity

AAPA-P2-based ABPP experiment was utilized for site-specific analysis of acrylamide modification in BV-2 cells (Fig. 4B). The AAPA-P2-modified peptides were enriched and released for LC-MS/MS analysis. 915 AAPA-P2-modified peptides from 754 proteins were identified in all the three biological replicates (Fig. 5A). In addition, we identified 1260 cysteine as well as 71 histidine and 42 tyrosine sites with AAPA-P2 modification (Fig. 5B and Supplementary Table S7). 313 proteins with two or more modified cysteine sites were identified as heavily-modified acrylamide targets (Fig. 5C), which were significantly enriched in biological processes, especially in neuroimmune system (Fig. 5D). Of the 238 high-sensitive proteins screened above, 96 were included in these 313 heavily-modified proteins (Fig. 5E). KEGG and GO analysis were performed on these 96 proteins. GO analysis revealed that these proteins are mainly distributed in cellular components such as cytoplasm and mitochondria (Supplementary Fig. S12A) and are involved in translation, cellular response to interleukin-7 and other biological processes (Supplementary Fig. S12B). These proteins also have many molecular functions, such as RNA binding and nucleic acid binding (Supplementary Fig. S12C). Interestingly, these 96 proteins contained key proteins involved in ubiquitin-protease system, mitochondria and cell death, suggesting AA may regulate neurotoxicity through related pathways (Fig. 5F). KEGG analysis revealed that these 96 proteins were mainly involved in ferroptosis, metabolic pathways and Parkinson's pathway (Supplementary Fig. S12D). For example, glutathione peroxidase 4 (GPX4), a highly sensitive and highly modified protein screened experimentally, is a key protein for iron death and one of the key target proteins in neurodegenerative disease Alzheimer's disease. In addition, we found that acrylamide may covalently bind calcium ion channel proteins, VDAC2 (voltage-dependent anion channel 2) and VDAC3 (voltage-dependent anion channel 3), which happen to be involved in iron death and Parkinson's disease pathways (Supplementary Table S8).

For validation, two proteins associated with neuroinflammation,

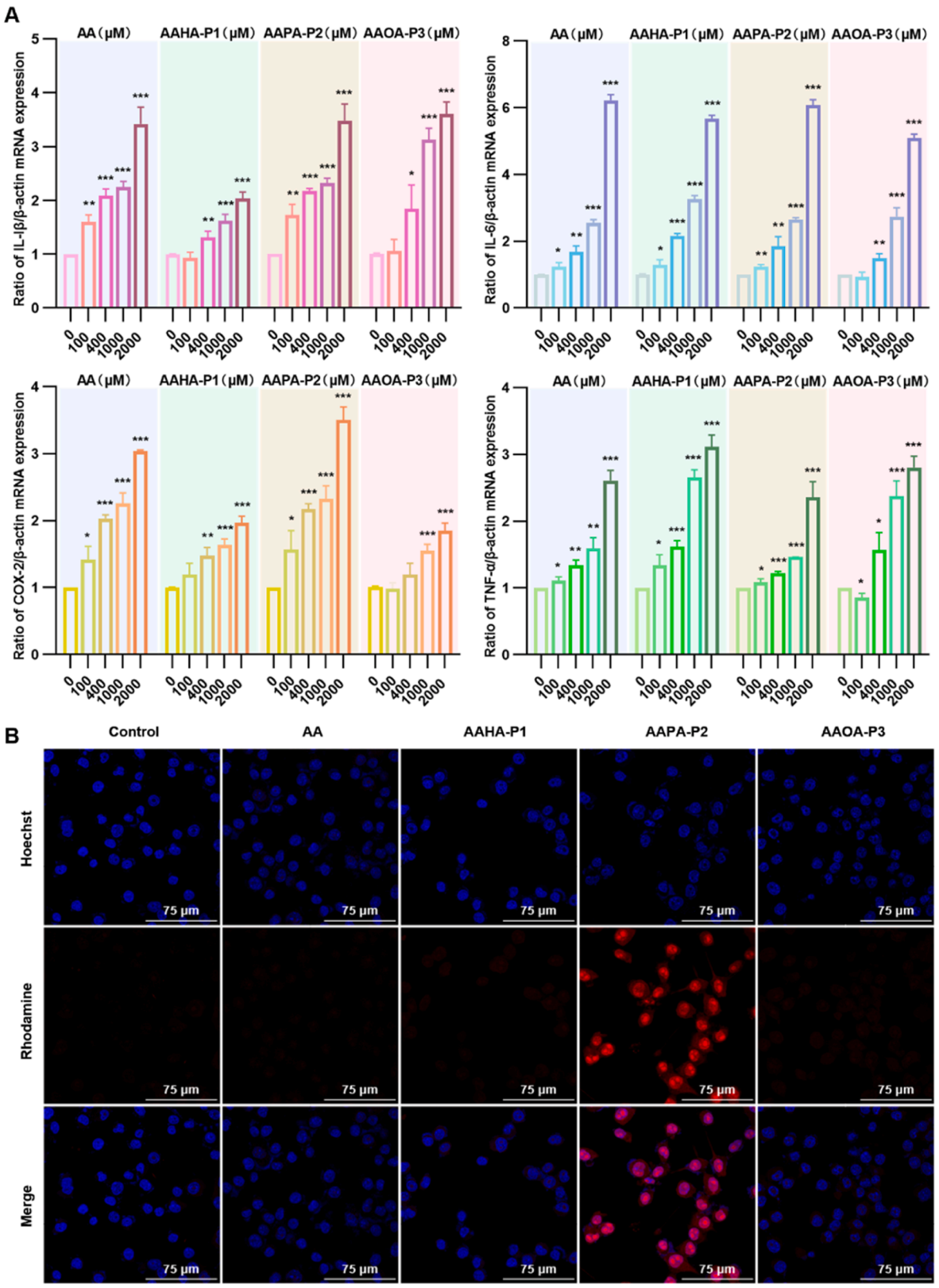

Fig. 2. The biofunctional comparability between probes and acrylamide and the ability of probes to label target proteins in living BV-2 cells were studied. (A) Probes recapitulate the biological function of AA. AA and three probes significantly induce TNF-α, IL-6, IL-1β, and COX-2 secretion in BV-2 cells. BV-2 cells were treated with 100, 400, 1000, and 2000 μM of AA and three probes for 24 h, respectively. The mRNA level of IL-1β, IL-6, TNF-α, and COX-2 in AA, AAHA-P1, AAPA-P2, or AAOA-P3-stimulated BV-2 cells were quantified by qPCR. All data are shown as mean ± SD (n = 3), * $p < 0.05$, * * $p < 0.01$, * ** $p < 0.001$, unpaired *t*-test. (B) Probes label target proteins in living BV-2 cells. BV-2 cells labeled with 1000 μM AAHA-P1, AAPA-P2, or AAOA-P3 by incubating 24 h were fixed and reacted with 50 μM Rhodamine-azide, followed by Hoechst 33342 and then imaged by fluorescence confocal microscopy.

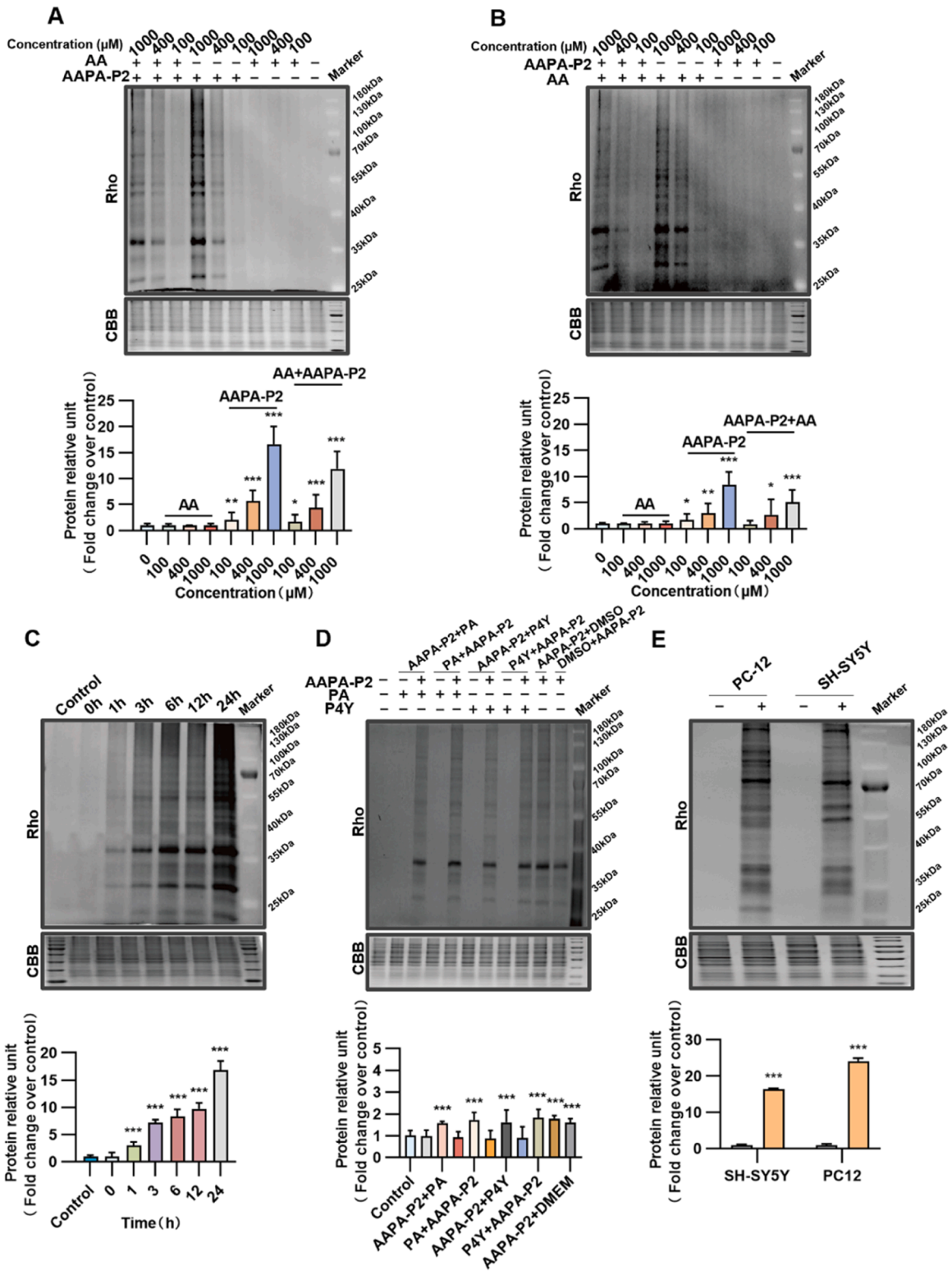

Fig. 3. The covalent binding similarity between AAPA-P2 and acrylamide were studied. (A) Competitive labeling of AA by AAPA-P2 in living BV-2 cells. BV-2 cells were pre-treated with 100, 400 and 1000 μM AA, respectively. Then the cells were separately labeled with 100, 400 and 1000 μM AAPA-P2. (B) Competitive labeling of AAPA-P2 by AA in living BV-2 cells. BV-2 cells were pre-treated with 100, 400, 1000 μM AAPA-P2, respectively. Then the cells were separately labeled with 100, 400 and 1000 μM AA. (C) Time-dependent labeling of AAPA-P2 in living BV-2 cells. (D) Competitive labeling of P2 by propionamide (PA) or pent-4-ynamide (P4Y) in living BV-2 cells. BV-2 cells were treated with 1000 μM AAPA-P2 for different time points. (E) Evaluation of AAPA-P2 labeling in multiple cell types, including SH-SY5Y and PC12 cells. Gels shown in the right side are representative blots from three biologically dependent samples per group, and bands were quantified using ImageJ. All data are shown as mean ± SD (n = 3), * $p < 0.05$, * * $p < 0.01$, * ** $p < 0.001$, unpaired *t*-test.

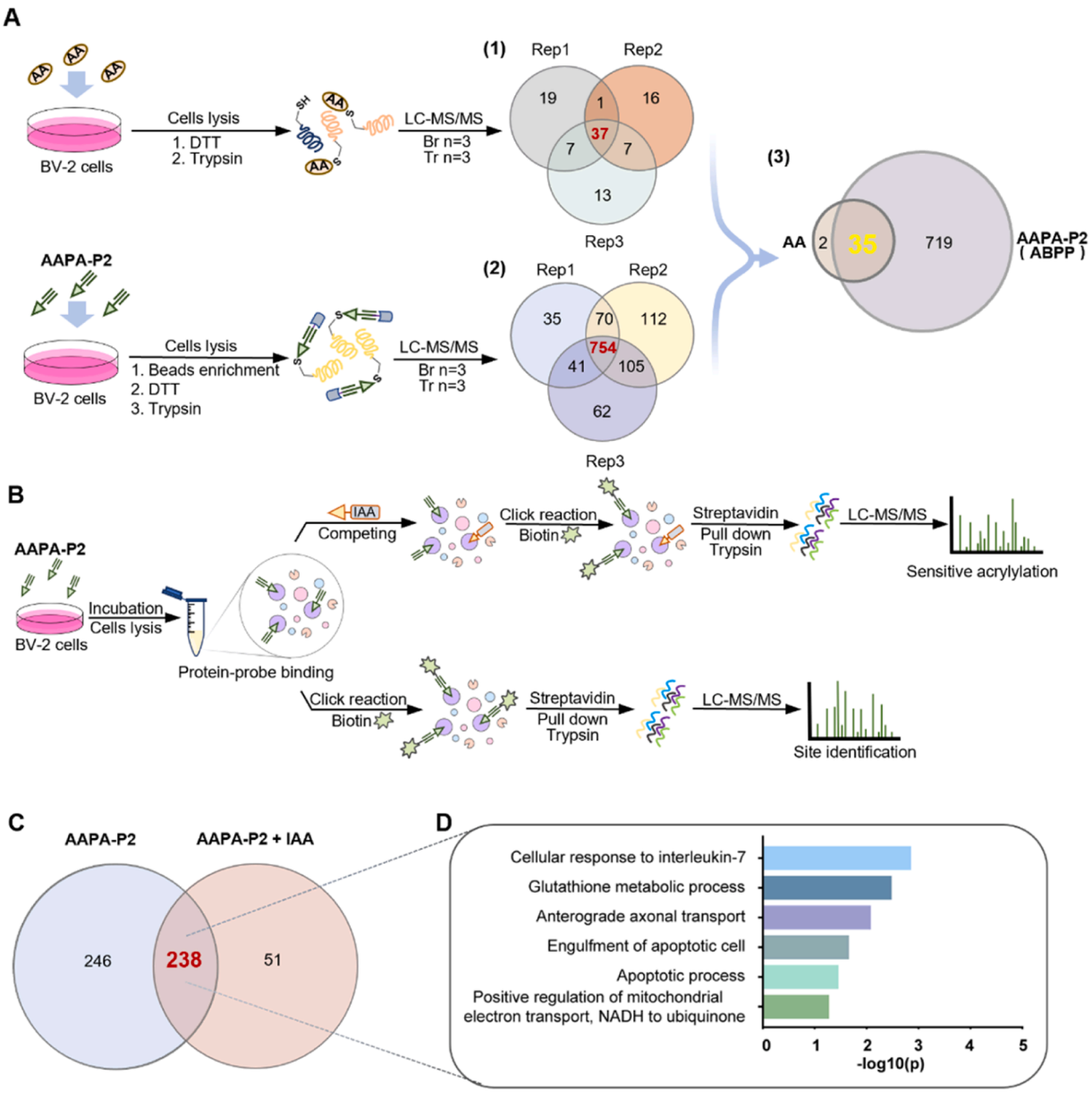

Fig. 4. Proteomics profiling of AA and AAPA-P2 modified peptides in BV-2 cells. (A) Proteomics analysis of the acrylamide targets in BV-2 cells: (1) Overlap of AA-modified proteins in three biological replicates; (2) Overlap of AAPA-P2-modified proteins in three biological replicates; (3) Overlap of AA and AAPA-P2-modified proteins in BV-2cells. (B) Workflow for high-sensitive chemoproteomic and site-specific chemoproteomic profiling of acrylylation in microlia cells. (C) Overlap of the AAPA-P2-modified proteins competed with 20 μM IAA in three biological replicates. (D) Biological analysis of 238 targets obtained in (C).

ANXA1 and TPI1, which are among the 96 proteins screened above, were overexpressed in BV-2 cells, and then the cells were treated with 1000 μM AAPA-P2 for 24 h, respectively. After conjugation with azide-biotin, the lysates were analyzed by immunoblotting before or after streptavidin enrichment. Both two proteins were successfully captured by AAPA-P2 (Fig. 5G).

Next, two novel targets, PSMD9 and NDUFA5, were overexpressed in BV-2 cells and the identified cysteine binding sites therein were mutated. The C59 of PSMD9 was mutated to C59S, and the mutated site was found to completely abolish the AAPA-P2 labeling on PSMD9, demonstrating that AAPA-P2 is covalently bound to C59 of PSMD9 (Fig. 5H and Supplementary Fig. S11A). Similarly, mutation of the C17 of NDUFA5 to C17S abolished the characteristic modification of AAPA-P2 on NDUFA5 (Fig. 5I and Supplementary Fig. S11B). Using the MST method, the dissociation constants (K_D) of AA were determined to be 81.97 ± 58.29 μM with PSMD9 and 7.86 ± 7.32 nM with NDUFA5 (Fig. 5J-K), which further confirmed the interaction of AA with PSMD9 and NDUFA5.

3.5. The crosstalk between the acrylation of PSMD9 and NDUFA5 induces mitochondrial activation of neuronal apoptotic mechanisms

Label-free quantitative proteomic analysis of proteins was performed on proteins enriched by the AAPA-P2 probe, and relevant proteins with significantly altered expression levels in the proteasome-mitochondrial induced apoptosis pathway were identified (Supplementary Table S9). Then several of these proteins associated with the ubiquitin-proteasome system as well as the mitochondrial ATP production system, including α-synuclein, VDAC1 and caspase-3, were evaluated by IF and WB. The results of IF experiments showed that the expression of α-synuclein, which is regulated by PSMD9, was significantly upregulated in cytosolic cells 24 h after administration of 1 mM AA to BV-2 cells (Fig. 6A). Since

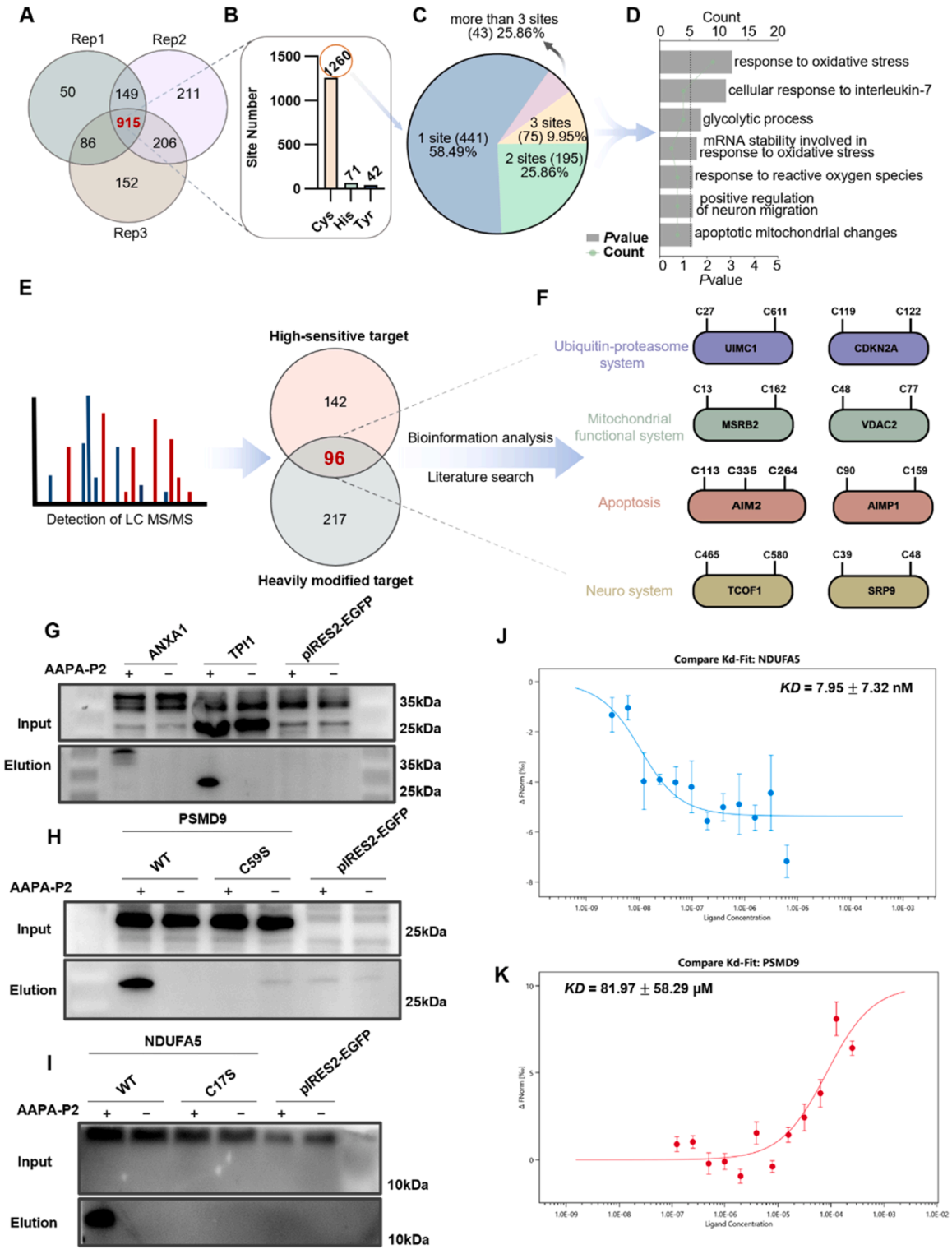

Fig. 5. Proteomic and checkpoint-specific analysis of key acrylated targets in BV-2 cells and verification of their checkpoint binding. (A) Overlap of the acrylamide modified peptide identified by AAPA-P2 in three biological replicates. (B) Number of the acrylamide cysteines, histidines and tyrosines identified from the tandem orthogonal proteolysis-activity-based protein (TOP-ABPP) profiling. (C) Distribution of the acrylylation targets by number of the cysteine modification sites. (D) Biological process analysis of the targets with heavily-modified acrylylation. (E) Overlap of high sensitive and heavily modified proteins. (F) Pathway analysis of the protein targets with multiple acrylamide sites. (G) Validation of AAPA-P2 labeling on known AA targets, including ANXA1 and TPI1. (H-I) Validation of AAPA-P2 labeling on novel AA targets, including PSMD9 and NDUFA5. (J-K) MST analysis of interactions between AA and His-PSMD9 and NDUFA5. The data were derived from the effect of AA on the fluorescence decay or enhance of two proteins. The results were obtained from 3 parallel experiments (n = 3).

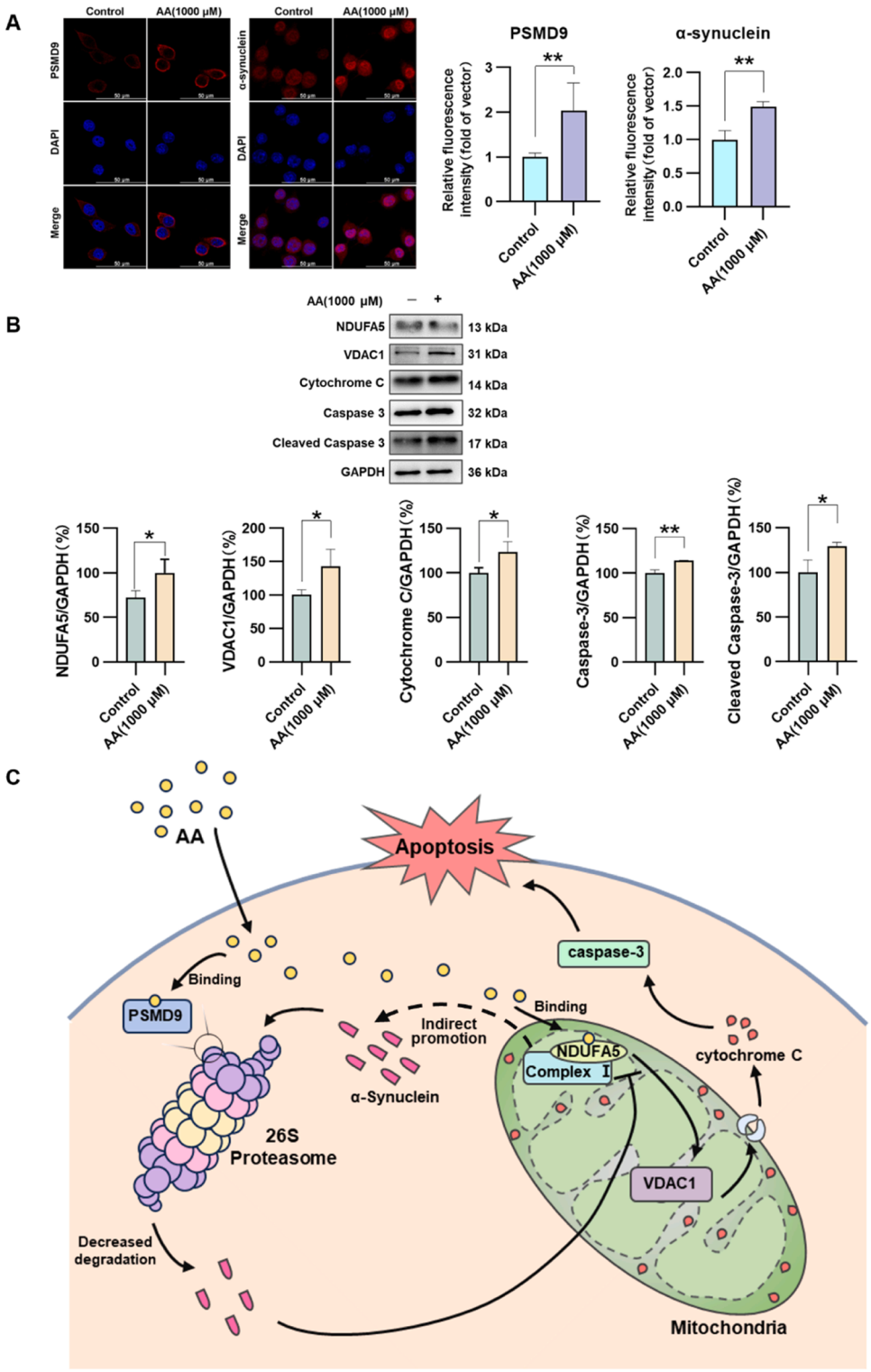

Fig. 6. Validation of the possible mechanism of AA neurotoxicity on BV-2 cells via new targets PSMD9 and NDUFA5. (A) IF and statistical results of α-Synuclein and PSMD9. (C) WB results and statistical results of NDUFA5, Cytochrome C, Caspase-3, cleaved Caspase-3 and VDAC1. (C) Possible mechanism of AA triggering apoptosis in BV-2 Cells via PSMD9 and NDUFA5. All data are shown as mean ± SEM (n = 3), * $p < 0.05$, * * $p < 0.01$, * ** $p < 0.001$, unpaired *t*-test.

AA reduced the expression of NDUFA5 on mitochondrial complex 1, the expression of downstream VDAC1 protein increases, which in turn promotes the efflux of cytochrome C from mitochondria, eventually leading to a significant increase in caspase-3 and cleaved caspase-3 (Fig. 6A-B and Supplementary Fig. S11C).

By constructing cell lines overexpressing PSMD9 plasmid (overexpression, OE) and NDUFA5 (OE) through transfection, we aimed to further elucidate the molecular mechanisms by which PSMD9 and NDUFA5 induce apoptosis in BV-2 cells. It was found that in the over-expression groups transfected with PSMD9 or NDUFA5 plasmids, AA significantly promoted apoptosis in NDUFA5 (OE) cells compared to the Vector group, while the effect on PSMD9 (OE) cells was not significant

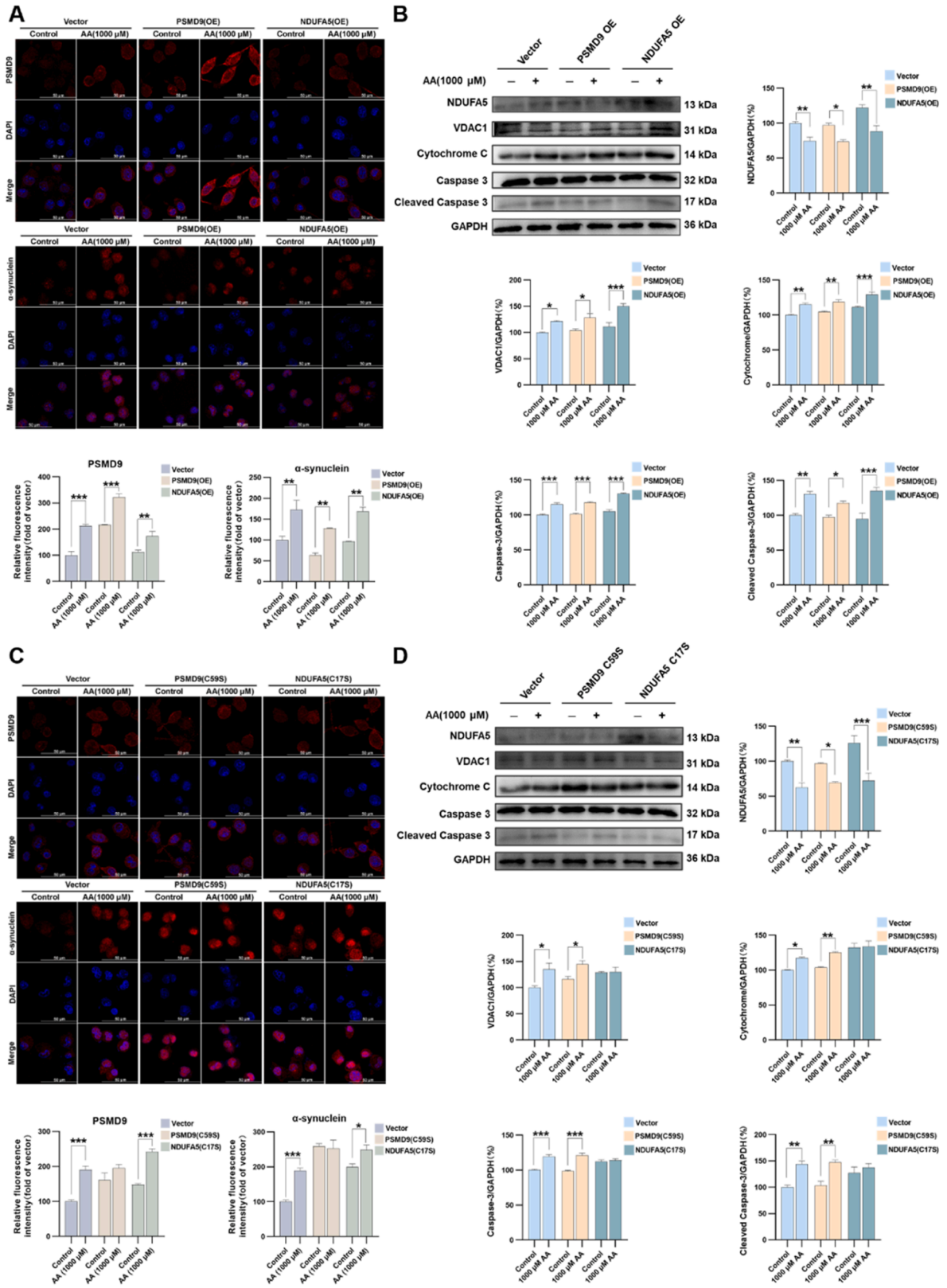

Fig. 7. AA triggers BV-2 cell apoptosis by binding PSMD9 to NDUFA5. (A) IF and statistical results of α-Synuclein and PSMD9, transfected with plasmid of PSMD9 (OE) or NDUFA5 (OE) and Vector. (B) WB results and statistical results of Cytochrome C, Caspase-3, cleaved Caspase-3, NDUFA5 and VDAC1, transfected with plasmid of PSMD9 (OE) or NDUFA5 (OE) and Vector. (C) IF and statistical results of α-Synuclein and PSMD9, transfected with plasmid of PSMD9 (C59S) or NDUFA5 (C17S) and Vector. (D) WB results and statistical results of Cytochrome C, Caspase-3, cleaved Caspase-3, NDUFA5 and VDAC1, transfected with plasmid of PSMD9 (C59S) or NDUFA5 (C59S) and Vector. Possible mechanism of AA triggering apoptosis in BV-2 Cells via PSMD9 and NDUFA5. All data are shown as mean ± SEM (n = 3), * $p < 0.05$, * * $p < 0.01$, * ** $p < 0.001$, Two-Way ANOVA.

(Fig. 7A-B). Based on these results, we speculated that the binding of AA to NDUFA5 is more likely to activate the Caspase-3-dependent apoptotic pathway.

Notably, in cells transfected with the mutant plasmid, we found that the expression level of α-synuclein in the control group of NDUFA5 (C17S) cells was significantly higher than that in the vector cells (Fig. 7D). This result is consistent with recent studies concluding that mitochondrial dysfunction can induce Parkinson's disease, and NDUFA5 is closely related to the activity of mitochondrial complex I [26,27]. Therefore, we speculate that the mutation of the unique cysteine site C17 on NDUFA5, which can bind with AA, affects the physiological function of mitochondrial complex I. In the mutant cell line transfected with PSMD9 (C59S) or NDUFA5 (C17S) plasmids, the results showed that the toxic effect of AA on NDUFA5 (C17S) cells was indistinguishable from that of the control group, as the mutation at Cys17 made it difficult for AA to bind. For PSMD9 (C59S) cells and the vector group, the effects of AA neurotoxicity were only observed in the ubiquitination-proteasome system, with no differences in the downstream mitochondrial apoptotic pathways (Fig. 7C-D).

4. Discussion

In this study, three acrylamide-alkynes probes, AAHA-P1, AAPA-P2 and AAOA-P3, were designed and synthesized. Among them, AAHA-P1 contains a longer 7C-atom alkyne-based carbon chain to provide an ideal site for introducing the biorthogonal handle. However, it was found during the experiments that the longer carbon chain resulted in poor water solubility. Therefore, we shortened the length of alkyne tail from 7 to 3 carbons for enhancing the cell membrane permeability of the probe, yielding AAPA-P2. Additionally, we designed a third probe, AAOA-P3, where the alkyne tail was reduced from 7 to 6 carbons while introducing a hydrophilic group (-O-) on the carbon chain. The synthesis methods for these probes were convenient, fast and mild, allowing the products to be obtained within 12–16 h at room temperature.

Then, the similarity between the probes and AA was evaluated at both the chemical and cellular levels. By comparing the reactivity of the synthetic probes and AA with Cys residues, the functional similarity of the probes with AA in BV-2 cells, as well as the ability of the probes to specifically label acrylamide targets in living BV-2 cells, it was demonstrated that AAPA-P2 has the most similar target profile to AA and can serve as a suitable probe for profiling the "arylamidation" in the proteome of BV-2 cells. In contrast, AAHA-P1 and AAOA-P3 may be less suitable as probes for use in living cells due to their longer carbon chains, which could result in stronger hydrophobicity, making it difficult for them to penetrate the cell membrane. Moreover, AAPA-P2 could also label human neuroblastoma cells (SH-SY5Y) and rat pheochromocytoma cells (PC12) with similar efficiency, which have been commonly used to study neurotoxicity in previous works [28–31], indicating that the probe we designed and synthesized has broad applicability.

Multiple studies have reported that AA, due to its unique chemical structure, has strong nucleophilicity and readily binds to cysteine residues. Therefore, in addition to enriching target proteins with AAPA-P2, we also conducted direct chemical proteomics experiments to identify AA targets for comparison. The results showed that the number of proteins directly modified by AA is limited (37 proteins), which is comparable to the number detected by David S et al. in the rat brain (41 proteins) [32]. In contrast, the number of proteins that can be enriched by our synthesized probe is more than 20 times that of the proteins directly modified by AA. This result indicates that our designed probe significantly increases the number of potential AA target proteins that can be identified.

By combining AAPA-P2 with the ABPP technique [33–38], 754 target proteins were enriched from living cells, significantly increasing the number of identified target proteins. Most of AA-modified proteins were included in the target proteins enriched by AAPA-P2, indicating the probe's precise enrichment capability. Subsequently, 238 high-sensitivity target proteins were further screen out by IAA competitive experiment, and two of them, ANXA1 and TPI1, which are known to be associated with neurotoxicity [15,39], were selected for validation, demonstrating that AAPA-P2 can serve as a straightforward method to assist in the biochemical verification of AA on individual proteins of interest.

Additionally, among the screened target proteins, we found that AA can covalently modify Cys59 of PSMD9 on the proteasome and Cys17 of NDUFA5 on mitochondrial complex I, which have not been reported in previous literature. Therefore, we further explored the molecular mechanisms by which AA induces neurotoxicity through its binding to PSMD9 and NDUFA5. PSMD9 is part of the non-ATPase 19S proteasome subunit, which is critical for maintaining homeostasis in the ubiquitin-proteasome system and is involved in detoxification and targeting misfolded proteins, whose inactivation leads to ubiquitin-proteasome dysfunction, promotes nerve cell death, and induces neurotoxicity [40–46]. NDUFA5 participates in the assembly of mitochondrial respiratory chain complex 1, and its mutation or deficiency will affect the assembly and stability of the electron transfer Q module of mitochondrial respiratory chain complex 1 [47,48]. Interestingly, dysfunction of the ubiquitin-proteasome system triggers mitochondrial autophagy, apoptosis and neurotoxicity. Conversely, dysregulation of mitochondrial function can ubiquitinate proteins, reduce the activity of the ubiquitin-proteasome system, induce cell death and enhance neurotoxicity. Therefore, we speculate that the crosstalk between the acrylation of PSMD9 and NDUFA5 may be co-regulated by the ubiquitin-proteasome system and the mitochondrial ATP production system [27,49–54].

In our study of the neurotoxic mechanisms of AA on normal cells and cells overexpressing PSMD9 or NDUFA5, we found that when AA enters the cells, the proteasome subunit PSMD9 binds to it, resulting in a relative increase in α-synuclein levels. α-synuclein is regulated by the proteasome, so this upregulation affects the physiological activity of mitochondrial complex I. AA also binds to NDUFA5, an assembly component of mitochondrial complex I, affecting its functional activity. Impairment of mitochondrial complex I function indirectly leads to an increase in the level of α-Synuclein, creating a feedback loop that exacerbates the dysfunction of mitochondrial complex I. This, in turn, promotes the accumulation of the downstream protein VDAC1, leading to the release of cytochrome c from mitochondria and the initiation of the caspase-3 dependent apoptotic cell death program. Through mutational experiments in PSMD9/NDUFA5 cells, we demonstrated that NDUFA5 is a key target for AA in regulating mitochondrial-dependent apoptosis.

Although we identified the low-abundance targets of AA, PSMD9 and NDUFA5, using AAPA-P2 probe and validated their plausibility at the cellular level as far as possible, there are still some questions that have not yet been fully addressed, such as whether AA induces neuronal toxicity through these two targets or key proteins associated with them, or other novel key targets captured by the method established herein, via other signaling pathways (i.e., the iron death signaling pathway with high KEGG score in our experiments), all of which need to be further investigated in follow-up experiments.

5. Conclusion

In this study, we synthesized three biorthogonal probes with site-selective specificity and cell permeability similar to the structure of acrylamide. AAPA-P2 were selected by evaluation for subsequent chemical proteomics analysis of acrylamide targets in living cells. Using this probe, 754 acrylamide-modified proteins were captured and identified, which significantly improved the efficiency of protein identification compared with traditional proteomics. Among the 236 high-sensitivity proteins obtained from further screening, two potential new targets, PSMD9 and NDUFA5 were identified, both of which are associated with neurodegenerative diseases. AA can modulate the

ubiquitination-proteasome system and mitochondrial functional activity through crosstalk between these two targets, inducing caspase3-dependent apoptosis and triggering neurotoxicity Follow-up work will explore more potential targets of AA to further elucidate the mechanisms of AA neurotoxicity and its possible association with neurodegenerative diseases after long-term ingestion or occupational exposure, and to provide new potential therapeutic targets for acrylamide-induced neurotoxicity.

Environmental implication

Acrylamide is typically produced during the high-temperature cooking of starchy foods and is also widely used in the production of polyacrylamide for soil conditioning and wastewater treatment. Prolonged ingestion or Long-term occupational exposure to acrylamide can lead to various adverse health outcomes, the most common of which is neurotoxicity. However, the mechanism of acrylamide-induced neurotoxicity has not been clearly characterized due to the limited number of targets identified to date. Here, we synthesized a specific bioorthogonal probe and successfully captured more potential targets, providing in-depth insights into the molecular mechanisms by which AA-induced neurological damage.

CRediT authorship contribution statement

Jia Shang: Writing – review & editing. **Binru Zheng:** Writing – original draft, Formal analysis. **Qianqian Tao:** Methodology. **Yuanqing Wei:** Validation. **An Kang:** Data curation. **Jizhou Yin:** Software. **Rui Liu:** Validation. **Shuying Han:** Project administration, Conceptualization. **Hongzhen Lian:** Supervision.

Declaration of Competing Interest

The authors declare that they have no known competing financial interests or personal relationships that could have appeared to influence the work reported in this paper.

Acknowledgements

This research was supported by the National Natural Science Foundation of China (No. 82174090, 21874065, 22176085 and 82474055), Jiangsu Qinglan Project, Jiangsu “333″ Project the Open Project of Chinese Materia Medica First-Class Discipline of Nanjing University of Chinese Medicine (ZYXYL2024-011) and the Jiangsu Agricultural Science and Technology Innovation Fund (CX(22)3173).

Appendix A. Supporting information

Supplementary data associated with this article can be found in the online version at doi:10.1016/j.jhazmat.2024.136760.

Data Availability

Data will be made available on request.

References

[1] Koszucka, A., Nowak, A., Nowak, I., Motyl, I., 2020. Acrylamide in human diet, its metabolism, toxicity, inactivation and the associated European Union legal regulations in food industry. Crit Rev Food Sci Nutr 60, 1677–1692. https://doi.org/10.1080/10408398.2019.1588222.

[2] Lopachin, R.M., Gavin, T., Barber, D.S., 2008. Type-2 alkenes mediate synaptotoxicity in neurodegenerative diseases. Neurotoxicology 29, 871–882. https://doi.org/10.1016/j.neuro.2008.04.016.

[3] Matoso, V., Bargi-Souza, P., Ivanski, F., Romano, M.A., Romano, R.M., 2019. Acrylamide: a review about its toxic effects in the light of Developmental Origin of Health and Disease (DOHaD) concept. Food Chem 283, 422–430. https://doi.org/10.1016/j.foodchem.2019.01.054.

[4] Reynolds, T., 2002. Acrylamide and cancer: tunnel leak in Sweden prompted studies. J Natl Cancer Inst 94, 876–878. https://doi.org/10.1093/jnci/94.12.876.

[5] Wang, X., Tang, B., Bao, L., Zhang, H., He, M., Yuan, S., 2022. Degradation evaluation of acrylamide in advanced oxidation processes based on theoretical method: mechanisms, kinetics, toxicity evaluation and the role of soil particles. J Hazard Mater 424, 127592. https://doi.org/10.1016/j.jhazmat.2021.127592.

[6] Zhang, Y., Xie, J., 2024. Ferroptosis implication in environmental-induced neurotoxicity. Sci Total Environ 934, 172618. https://doi.org/10.1016/j.scitotenv.2024.172618.

[7] Friedman, M., 2003. Chemistry, biochemistry, and safety of acrylamide. A review. J Agric Food Chem 51, 4504–4526. https://doi.org/10.1021/jf030204.

[8] Mihalache, O.A., Dall’Asta, C., 2024. The burden of disease due to dietary exposure to acrylamide in Italy: a risk assessment-based approach. Food Chem Toxicol 188, 114699. https://doi.org/10.1016/j.fct.2024.114699.

[9] Yu, Y., Zhang, D., Xu, J., Zhang, D., Yang, L., Xia, R., et al., 2023. Adolescence is a sensitive period for acrylamide-induced sex hormone disruption: evidence from NHANES populations and experimental mice. Ecotoxicol Environ Saf 249, 114413. https://doi.org/10.1016/j.ecoenv.2022.114413.

[10] Guo, J., Garshick, E., Si, F., Tang, Z., Lian, X., Wang, Y., et al., 2024. Environmental toxicant exposure and depressive symptoms. JAMA Netw Open 7, e2420259. https://doi.org/10.1001/jamanetworkopen.2024.20259.

[11] LoPachin, R.M., Barber, D.S., 2006. Synaptic cysteine sulfhydryl groups as targets of electrophilic neurotoxicants. Toxicol Sci 94, 240–255. https://doi.org/10.1093/toxsci/kfl066.

[12] Lopachin, R.M., Decaprio, A.P., 2005. Protein adduct formation as a molecular mechanism in neurotoxicity. Toxicol Sci 86, 214–225. https://doi.org/10.1093/toxsci/kfi197.

[13] LoPachin, R.M., Barber, D.S., Gavin, T., 2008. Molecular mechanisms of the conjugated α,β-unsaturated carbonyl derivatives: relevance to neurotoxicity and neurodegenerative diseases. Toxicol Sci 104, 235–249. https://doi.org/10.1093/toxsci/kfm301.

[14] Qin, W., Zhang, Y., Tang, H., Liu, D., Chen, Y., Liu, Y., et al., 2020. Chemoproteomic profiling of itaconation by bioorthogonal probes in inflammatory macrophages. J Am Chem Soc 142, 10894–10898. https://doi.org/10.1021/jacs.9b11962.

[15] Wang, F., Fan, B., Chen, C., Zhang, W., 2022. Acrylamide causes neurotoxicity by inhibiting glycolysis and causing the accumulation of carbonyl compounds in BV2 microglial cells. Food Chem Toxicol 163, 112982. https://doi.org/10.1016/j.fct.2022.112982.

[16] Pernice, R., Hauder, J., Koehler, P., Vitaglione, P., Fogliano, V., Somoza, V., 2009. Effect of sulforaphane on glutathione-adduct formation and on glutathione-S-transferase-dependent detoxification of acrylamide in Caco-2 cells. Mol Nutr Food Res 53, 1540–1550. https://doi.org/10.1002/mnfr.200900447.

[17] Zhu, F., Wang, J., Jiao, J., Zhang, Y., 2021. Exposure to acrylamide induces skeletal developmental toxicity in zebrafish and rat embryos. Environ Pollut 271, 116395. https://doi.org/10.1016/j.envpol.2020.116395.

[18] Raldúa, D., Casado, M., Prats, E., Faria, M., Puig-Castellví, F., Pérez, Y., et al., 2020. Targeting redox metabolism: the perfect storm induced by acrylamide poisoning in the brain. Sci Rep 10, 312. https://doi.org/10.1038/s41598-019-57142-y.

[19] Wang, A., Wan, X., Zhuang, P., Jia, W., Ao, Y., Liu, X., et al., 2023. High fried food consumption impacts anxiety and depression due to lipid metabolism disturbance and neuroinflammation. Proc Natl Acad Sci USA 120, e2221097120. https://doi.org/10.1073/pnas.2221097120.

[20] Zhang, B., Zhao, M., Ji, X., Xia, Q., Jiang, L., Zhao, L., 2023. Acrylamide induces neurotoxicity in zebrafish (Danio rerio) via NLRP3-mediated pyroptosis. Sci Total Environ 896, 165208. https://doi.org/10.1016/j.scitotenv.2023.165208.

[21] Martyniuk, C.J., Feswick, A., Fang, B., Koomen, J.M., Barber, D.S., Gavin, T., et al., 2013. Protein targets of acrylamide adduct formation in cultured rat dopaminergic cells. Toxicol Lett 219, 279–287. https://doi.org/10.1016/j.toxlet.2013.03.031.

[22] Barber, D.S., Stevens, S., LoPachin, R.M., 2007. Proteomic analysis of rat striatal synaptosomes during acrylamide intoxication at a low dose rate. Toxicol Sci 100, 156–167. https://doi.org/10.1093/toxsci/kfm210.

[23] Cravatt, B.F., Wright, A.T., Kozarich, J.W., 2008. Activity-based protein profiling: from enzyme chemistry to proteomic chemistry. Annu Rev Biochem 77, 383–414. https://doi.org/10.1146/annurev.biochem.75.101304.124125.

[24] Zhang, Q., Luo, P., Chen, J., Yang, C., Xia, F., Zhang, J., et al., 2022. Dissection of targeting molecular mechanisms of aristolochic acid-induced nephrotoxicity via a combined deconvolution strategy of chemoproteomics and metabolomics. Int J Biol Sci 18, 2003–2017. https://doi.org/10.7150/ijbs.69618.

[25] Böttcher, T., Pitscheider, M., Sieber, S.A., 2010. Natural products and their biological targets: proteomic and metabolomic labeling strategies. Angew Chem Int Ed Engl 49, 2680–2698. https://doi.org/10.1002/anie.200905352.

[26] Vos, M., 2022. Mitochondrial complex I deficiency: guilty in Parkinson’s disease. Signal Transduct Target Ther 7, 136. https://doi.org/10.1038/s41392-022-00983-3.

[27] Nie, H., Yu, X., He, H., Zhou, L., Li, Q., Song, C., et al., 2018. Hepatocyte miR-33a mediates mitochondrial dysfunction and hepatosteatosis by suppressing NDUFA5. J Cell Mol Med 22, 6285–6293. https://doi.org/10.1111/jcmm.13918.

[28] Martínez, M.A., Rodríguez, J.L., Lopez-Torres, B., Martínez, M., Martínez-Larrañaga, M.R., Maximiliano, J.E., et al., 2020. Use of human neuroblastoma SH-SY5Y cells to evaluate glyphosate-induced effects on oxidative stress, neuronal development and cell death signaling pathways. Environ Int 135, 105414. https://doi.org/10.1016/j.envint.2019.105414.

[29] Zhao, Q., Tian, Z., Zhou, G., Niu, Q., Chen, J., Li, P., et al., 2020. SIRT1-dependent mitochondrial biogenesis supports therapeutic effects of resveratrol against

neurodevelopment damage by fluoride. Theranostics 10, 4822–4838. https://doi.org/10.7150/thno.42387.
[30] Tang, H., Huang, H., Wang, D., Li, P., Tian, Z., Li, D., et al., 2022. TFEB ameliorates autophagy flux disturbance induced by PBDE-47 via up-regulating autophagy-lysosome fusion. J Hazard Mater 430, 128483. https://doi.org/10.1016/j.jhazmat.2022.128483.
[31] Chen, Y., Xie, H.Q., Sha, R., Xu, T., Zhang, S., Fu, H., et al., 2020. 2,3,7,8-Tetrachlorodibenzo-p-dioxin and up-regulation of neurofilament expression in neuronal cells: evaluation of AhR and MAPK pathways. Environ Int 134, 105193. https://doi.org/10.1016/j.envint.2019.105193.
[32] Barber, D.S., LoPachin, R.M., 2004. Proteomic analysis of acrylamide-protein adduct formation in rat brain synaptosomes. Toxicol Appl Pharm 201, 120–136. https://doi.org/10.1016/j.taap.2004.05.008.
[33] Yashkin, A., Rayo, J., Grimm, L., Welch, M., Meijler, M.M., 2021. Short-chain reactive probes as tools to unravel the Pseudomonas aeruginosa quorum sensing regulon. Chem Sci 12, 4570–4581. https://doi.org/10.1039/d0sc04444j.
[34] McCloud, R.L., Yuan, K., Mahoney, K.E., Bai, D.L., Shabanowitz, J., Ross, M.M., et al., 2021. Direct target site identification of a sulfonyl-triazole covalent kinase probe by LC-MS chemical proteomics. Anal Chem 93, 11946–11955. https://doi.org/10.1021/acs.analchem.1c01591.
[35] Koo, T.Y., Lai, H., Nomura, D.K., Chung, C.Y., 2023. N-Acryloylindole-alkyne (NAIA) enables imaging and profiling new ligandable cysteines and oxidized thiols by chemoproteomics. Nat Commun 14, 3564. https://doi.org/10.1038/s41467-023-39268-w.
[36] Zhang, Q., Luo, P., Zheng, L., Chen, J., Zhang, J., Tang, H., et al., 2022. 18beta-glycyrrhetinic acid induces ROS-mediated apoptosis to ameliorate hepatic fibrosis by targeting PRDX1/2 in activated HSCs. J Pharm Anal 12, 570–582. https://doi.org/10.1016/j.jpha.2022.06.001.
[37] Hong, Z., Cao, J., Liu, D., Liu, M., Chen, M., Zeng, F., et al., 2023. Celastrol targeting Nedd4 reduces Nrf2-mediated oxidative stress in astrocytes after ischemic stroke. J Pharm Anal 13, 156–169. https://doi.org/10.1016/j.jpha.2022.12.002.
[38] Wei, W., Zeng, Q., Wang, Y., Guo, X., Fan, T., Li, Y., et al., 2023. Discovery and identification of EIF2AK2 as a direct key target of berberine for anti-inflammatory effects. Acta Pharm Sin B 13, 2138–2151. https://doi.org/10.1016/j.apsb.2022.12.009.
[39] Solito, E., McArthur, S., Christian, H., Gavins, F., Buckingham, J.C., Gillies, G.E., 2008. Annexin A1 in the brain-undiscovered roles? Trends Pharm Sci 29, 135–142. https://doi.org/10.1016/j.tips.2007.12.003.
[40] Alam, M.M., Yang, D., Li, X.Q., Liu, J., Back, T.C., Trivett, A., et al., 2022. Alpha synuclein, the culprit in Parkinson disease, is required for normal immune function. Cell Rep 38, 110090. https://doi.org/10.1016/j.celrep.2021.110090.
[41] Dehay, B., Bourdenx, M., Gorry, P., Przedborski, S., Vila, M., Hunot, S., et al., 2015. Targeting α-synuclein for treatment of Parkinson's disease: mechanistic and therapeutic considerations. Lancet Neurol 14, 855–866. https://doi.org/10.1016/s1474-4422(15)00006-x.
[42] Meul, T., Berschneider, K., Schmitt, S., Mayr, C.H., Mattner, L.F., Schiller, H.B., et al., 2020. Mitochondrial regulation of the 26S proteasome. Cell Rep 32, 108059. https://doi.org/10.1016/j.celrep.2020.108059.
[43] Kodroń, A., Mussulini, B.H., Pilecka, I., Chacińska, A., 2021. The ubiquitin-proteasome system and its crosstalk with mitochondria as therapeutic targets in medicine. Pharm Res 163, 105248. https://doi.org/10.1016/j.phrs.2020.105248.
[44] Puerta, E., Hervias, I., Goñi-Allo, B., Zhang, S.F., Jordán, J., Starkov, A.A., et al., 2010. Methylenedioxymethamphetamine inhibits mitochondrial complex I activity in mice: a possible mechanism underlying neurotoxicity. Br J Pharm 160, 233–245. https://doi.org/10.1111/j.1476-5381.2010.00663.x.
[45] Yang, W., Cui, H., Chai, Z., Zou, P., Shi, F., Yang, B., et al., 2022. Benzo[a]pyrene inhibits testosterone biosynthesis via NDUFA10-mediated mitochondrial compromise in mouse Leydig cells: Integrating experimental and in silico toxicological approaches. Ecotoxicol Environ Saf 244, 114075. https://doi.org/10.1016/j.ecoenv.2022.114075.
[46] Christie, J., Anthony, C.M., Harish, M., Mudartha, D., Ud, Din, Farooqee, S.B., et al., 2023. The interaction network of the proteasome assembly chaperone PSMD9 regulates proteostasis. FEBS J 290, 5581–5604. ⟨https://doi:10.1111/febs.16948⟩.
[47] Peralta, S., Torraco, A., Wenz, T., Garcia, S., Diaz, F., Moraes, C.T., 2014. Partial complex I deficiency due to the CNS conditional ablation of Ndufa5 results in a mild chronic encephalopathy but no increase in oxidative damage. Hum Mol Genet 23, 1399–1412. https://doi.org/10.1093/hmg/ddt526.
[48] Rak, M., Rustin, P., 2014. Supernumerary subunits NDUFA3, NDUFA5 and NDUFA12 are required for the formation of the extramembrane arm of human mitochondrial complex I. FEBS Lett 588, 1832–1838. https://doi.org/10.1016/j.febslet.2014.03.046.
[49] Lashuel, H.A., Overk, C.R., Oueslati, A., Masliah, E., 2013. The many faces of α-synuclein: from structure and toxicity to therapeutic target. Nat Rev Neurosci 14, 38–48. https://doi.org/10.1038/nrn3406.
[50] Lackie, R.E., de, Miranda, A.S., Lim, M.P., Novikov, V., Madrer, N., Karunatilleke, N.C., et al., 2022. Stress-inducible phosphoprotein 1 (HOP/STI1/STIP1) regulates the accumulation and toxicity of α-synuclein in vivo. Acta Neuropathol 144, 881–910. https://doi.org/10.1007/s00401-022-02491-8.
[51] Ludtmann, M.H.R., Angelova, P.R., Horrocks, M.H., Choi, M.L., Rodrigues, M., Baev, A.Y., et al., 2018. α-synuclein oligomers interact with ATP synthase and open the permeability transition pore in Parkinson's disease. Nat Commun 9, 2293. https://doi.org/10.1038/s41467-018-04422-2.
[52] Malpartida, A.B., Williamson, M., Narendra, D.P., Wade-Martins, R., Ryan, B.J., 2021. Mitochondrial dysfunction and mitophagy in Parkinson's disease: From mechanism to therapy. Trends Biochem Sci 46, 329–343. https://doi.org/10.1016/j.tibs.2020.11.007.
[53] Burté, F., De, Girolamo, L.A., Hargreaves, A.J., Billett, E.E., 2011. Alterations in the mitochondrial proteome of neuroblastoma cells in response to complex 1 inhibition. J Proteome Res 10, 1974–1986. https://doi.org/10.1021/pr101211k.
[54] Ramalingam, M., Jang, S., Hwang, J., Kim, B., Cho, H.H., Kim, E., et al., 2023. Neuroprotective effects of the neural-induced adipose-derived stem cell secretome against rotenone-induced mitochondrial and endoplasmic reticulum dysfunction. Int J Mol Sci 24, 5622. https://doi.org/10.3390/ijms24065622.